

# Journal of Materials Chemistry A

Accepted Manuscript



This is an *Accepted Manuscript*, which has been through the Royal Society of Chemistry peer review process and has been accepted for publication.

*Accepted Manuscripts* are published online shortly after acceptance, before technical editing, formatting and proof reading. Using this free service, authors can make their results available to the community, in citable form, before we publish the edited article. We will replace this *Accepted Manuscript* with the edited and formatted *Advance Article* as soon as it is available.

You can find more information about *Accepted Manuscripts* in the [Information for Authors](#).

Please note that technical editing may introduce minor changes to the text and/or graphics, which may alter content. The journal's standard [Terms & Conditions](#) and the [Ethical guidelines](#) still apply. In no event shall the Royal Society of Chemistry be held responsible for any errors or omissions in this *Accepted Manuscript* or any consequences arising from the use of any information it contains.

Cite this: DOI: 10.1039/c0xx00000x

[www.rsc.org/xxxxxx](http://www.rsc.org/xxxxxx)

Paper

## Spacer Effects in Metal-Free Organic Dyes for Visible-Light-Driven Dye-Sensitized Photocatalytic Hydrogen Production

Motonori Watanabe,<sup>\*a</sup> Hidehisa Hagiwara,<sup>a,b</sup> Aoi Iribe,<sup>b</sup> Yudai Ogata,<sup>b</sup> Kenta Shiomi,<sup>b</sup> Aleksandar Staykov,<sup>a</sup> Shintaro Ida,<sup>a,b</sup> Keiji Tanaka,<sup>a,b</sup> and Tatsumi Ishihara<sup>\*a,b</sup>

<sup>5</sup> Received (in XXX, XXX) XthXXXXXXXXXX 20XX, Accepted Xth XXXXXXXXXXXX 20XX

DOI: 10.1039/b000000x

Metal-free organic dyes containing benzo[*b*]phenothiazine were synthesized and effectively used for dye-sensitized visible-light-driven photocatalytic hydrogen production. The materials exhibited high stability and hydrogen production when numerous  $\pi$ -conjugated bridges were inserted as spacers between the donor and the anchor moiety. Photocatalytic hydrogen production was investigated in a TiO<sub>2</sub>/dye/Pt structure using triethanolamine as the sacrificial reagent. Compound dye **3**, which had the longest spacer between the donor and the acceptor, exhibited the best hydrogen production performance of the series examined in this study. It displayed a turnover number (TON) of 4460, a turnover frequency of 278 after 16 h, and a photo quantum efficiency of 1.65% at 420 nm. Furthermore, it showed the longest electron injection lifetime because its coordination structure was considered to be vertically standing on the TiO<sub>2</sub> surface by theoretical calculations. On the other hand, dye **1** showed the lowest hydrogen production performance with a TON of 483 and very short electron injection lifetime. This observation may suggest from the computation result, which showed the lying geometry of **1** with monodentate coordination of the dye with respect to the TiO<sub>2</sub> surface. This spacer effect–property relationship study may provide a good strategy for the development of metal-free organic dyes for dye-sensitized photocatalytic water splitting.

### Introduction

Production of hydrogen is the key to establishing clean energy systems, because hydrogen can be employed as a clean energy source in fuel cells.<sup>1</sup> Since the Honda–Fujishima water splitting effect using a rutile TiO<sub>2</sub> and a Pt black system was reported in 1972,<sup>2</sup> hydrogen gas production by photocatalytic water splitting has been investigated with TiO<sub>2</sub><sup>3,4</sup> and other semiconductors,<sup>5,6</sup> because it is one of the ideal hydrogen production methods. However, visible-light-driven photocatalytic water splitting is proven difficult to accomplish because almost all semiconductors have a wide band gap,<sup>5</sup> whereas a visible-light-driven photocatalyst requires a band gap of less than 3.0 eV ( $\lambda > 415$  nm).

<sup>†</sup> Electronic Supplementary Information (ESI) available: [reflectance and time-resolved absorption spectra, theoretical computation, and NMR spectra]. See DOI: 10.1039/b000000x/

Although some semiconductors have shown satisfactory visible-light-driven photocatalytic activity, many challenges still persist. These challenges include improving the water splitting efficiency and stability of catalysts through the engineering of semiconductors.<sup>5,7,8</sup> Alternatively, dye-sensitized photocatalytic water splitting systems may achieve hydrogen production under visible light.<sup>9,10</sup> Ruthenium complex dyes have displayed high efficiencies in dye-sensitized photocatalytic hydrogen production from water.<sup>11</sup> In particular, a dimer of ruthenium complex Ru<sub>2</sub>(bpy)<sub>4</sub>(BL)(ClO<sub>4</sub>)<sub>2</sub> showed good hydrogen production performance in a visible-light-driven Pt/dye/TiO<sub>2</sub> system with a turnover number (TON) of 75340 after 27 h.<sup>11b</sup> Other metal complex dyes, such as metal complex porphyrin (TON = 400), have also presented good hydrogen production rates.<sup>12</sup> These metal complex dyes benefit from metal-to-ligand charge transfer abilities, which enhance the electron injection rate from the dye to the semiconductor. A wide

<sup>a</sup>International Institute for Carbon-Neutral Energy Research (WPI-FCNER), Kyushu University, 744 Motooka, Nishi-ku, Fukuoka 819-0395 Japan.; E-mail: mwata@i2cner.kyushu-u.ac.jp

<sup>b</sup>Department of Applied Chemistry, Kyushu University, 744 Motooka, Nishi-ku, Fukuoka, 819-0395, Japan.

variety of organic dyes such as derivatives of coumarin,<sup>13a</sup> cyanine,<sup>13, 14</sup> xanthenes dyes,<sup>15</sup> imide<sup>16</sup> and 1,1'-bi-2-naphthol (BINOL) have been reported in the literature.<sup>17</sup> Compared to metal-containing materials, these dyes have the advantage of being environmentally friendly, abundant, cheap and flexible but have exhibited low hydrogen production rates (TON ~ 40) in similar Pt/dye/TiO<sub>2</sub> system. Performance enhancement of these metal-free complexes in water hinges on the design of new efficient sensitizers.

The environment between sensitizers and semiconductor surfaces has recently been reported to improve efficiency. Han *et al.* have demonstrated that hydrophilic substituents on sensitizers enhanced charge recombination lifetimes because aqueous media induced the relaxation of the dye from its excited state.<sup>18</sup> Lee *et al.* have reported that N-substitution by long alkyl chains improved the hydrogen productivity of phenothiazine derivatives by establishing a good electron injection pathway. These substituents changed the aggregation conformation of the dye on TiO<sub>2</sub> and/or prevented the undesired decomposition reaction in the excited state, resulting in a good performance of these metal-free dye systems (TON ~ 1026).<sup>19</sup> These results indicate that the selection of an appropriate dye structure can increase hydrogen production. Donor-spacer-acceptor dyad systems have exhibited remarkable quantum efficiency in dye-sensitized solar cells.<sup>20</sup> In these dyads, donor and spacer structures have played an important role in improving favourable electron injection into a semiconductor<sup>21,22</sup> and achieving a slow charge recombination between semiconductor and dye.<sup>23</sup>

In this study, the visible-light-driven photocatalytic activity of a novel donor-spacer-acceptor dye system was investigated with a focus on the relationship between hydrogen production and spacer length. The spacer can not only extend the absorption bands of visible light but also provide long charge recombination states by separating electron donor and acceptor sites. Substituents, such as hydrophilic groups, were introduced on the sensitizers to study the spacer effect. Benzo[*b*]phenothiazine was chosen as the electron donor because phenothiazine derivatives exhibit good electron donating ability and electrochemical stability in dye-sensitized solar cell systems.<sup>19,24</sup>

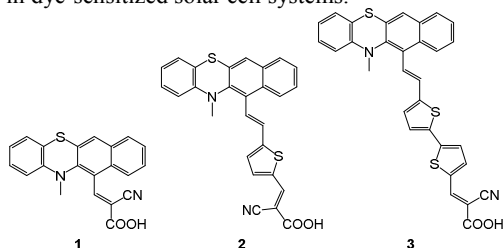


Figure 1. Series of synthesized dyes 1-3.

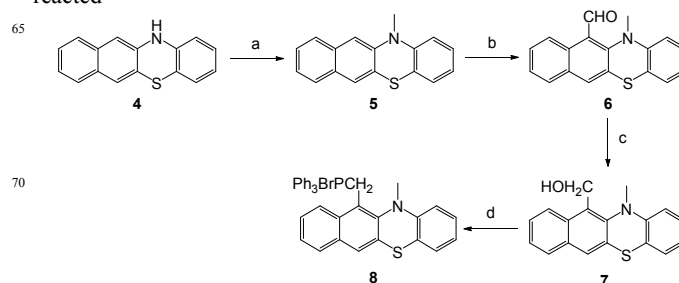
## Results and Discussion

### Synthesis

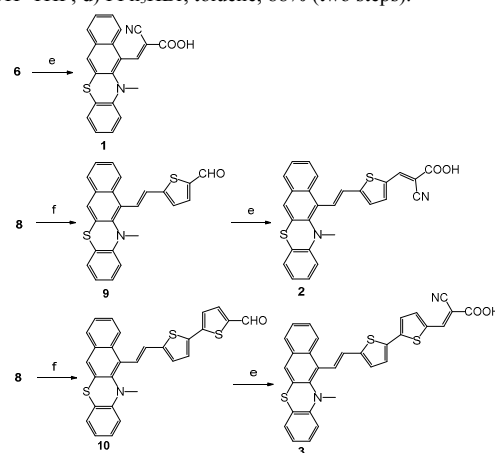
Dyes 1-3 were synthesized using benzo[*b*]phenothiazine (**4**) as the starting material. The secondary amine of **4** was methylated using an excess amount of MeI in K<sub>2</sub>CO<sub>3</sub>/THF. Formylation at the 11-position of the methylated compound (**5**) moiety by the Vilsmeier-Haack reaction produced aldehyde **6**. The reduction of **6** by NaBH<sub>4</sub> formed alcohol **7**, which was subsequently treated with triphenylphosphine hydrobromide to give the phosphonium

salt (**8**). Knoevenagel condensation of **8** with cyanoacetic acid afforded dye **1** in 48% yield. The cyanoacrylic acid moiety acted as the acceptor unit in dye **1**.

The distance between donor and acceptor was further elongated by addition of another aromatic moiety. The Wittig reagent (**8**) reacted



Scheme 1. Synthetic scheme for the preparation of aldehyde **6** and its phosphonium salt **8**. a) tBuOK, MeI, THF, 44%; b) POCl<sub>3</sub>, DMF, 78%; c) NaBH<sub>4</sub>, MeOH-THF; d) PPh<sub>3</sub>HBr, toluene, 88% (two steps).



Scheme 2. Synthetic scheme for the preparation of dyes 1-3. e) Cyanoacetic acid, NH<sub>4</sub>OAc, AcOH, 48%-75%; f) thiophene-2,5-dicarboxaldehyde or [2,2'-bithiophene]-5,5'-dicarbaldehyde, 18-crown-6, K<sub>2</sub>CO<sub>3</sub>, DMF, 50%-56%.

with thiophene-2,5-dicarboxaldehyde and [2,2'-bithiophene]-5,5'-dicarbaldehyde in the presence of 18-crown-6-ether to give aldehydes **9** and **10**, respectively, in 50%-56% yield. The presence of an aldehyde group in these intermediates was confirmed by the detection of <sup>1</sup>H NMR signals around 9.89-10.40 ppm. Similar to the synthesis of dye **1**, Knoevenagel condensation of these aldehydes with cyanoacetic acid produced the corresponding spacer-extended dyes **2** and **3** in 70%-75% yield. The <sup>13</sup>C NMR spectra of the final compounds displayed peaks at 163-164 ppm, indicating the presence of a carboxyl acid group. IR spectra also showed peaks at 1686-1693 cm<sup>-1</sup> which corresponded to the carboxylic acid group stretching bands. The formation of dyes **2** and **3** was further confirmed by HR-FAB-MS spectra.

### Physical Properties

The absorption spectra of organic dyes 1-3 in THF are shown in Fig. 2. Each compound displayed two major absorption bands at 250-330 nm and 350-550 nm. Short wavelength bands were assigned to π-π\* and n-π\*

transitions and long wavelength bands to internal charge-transfer (ICT) transitions. The ICT bands experienced a bathochromic shift with increasing number of thiophene spacers, i.e. **3** (443 nm) > **2** (391 nm) > **1** (363 nm). In addition, the ICT intensities increased with the number of thiophene spacers. Dyes **2** and **3** exhibited ICT excitation coefficients of 20312 nm/M<sup>-1</sup>cm<sup>-1</sup> and 22239 nm/M<sup>-1</sup>cm<sup>-1</sup>, respectively, indicating a significant electron interaction between the donor and the acceptor *via* the thiophene spacer moieties. On the other hand, the very weak excitation coefficient of **1** (5122 nm/M<sup>-1</sup>cm<sup>-1</sup>) may be explained by weak electron coupling interactions caused by steric hindrance from the N-methyl substituent.

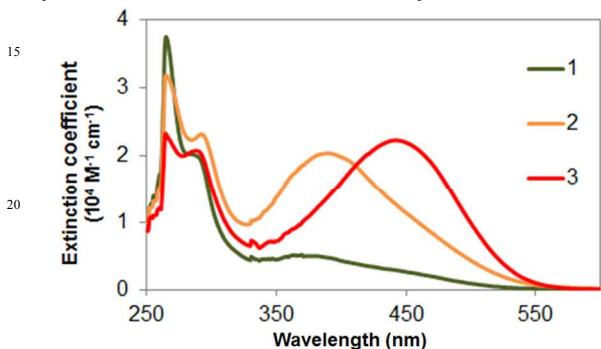


Figure 2. Absorption spectra of dyes **1–3** in THF ( $1.0 \times 10^{-4}$  M)

Dyes **1–3** presented similar absorption spectra on TiO<sub>2</sub> films as in THF, with the exception of a blue shift of *ca.* 20–30 nm for the ICT bands (Fig. 3 and Table 1). When the TiO<sub>2</sub> films **1–3** were measured in the THF, no shift of absorption was found (Fig. S2). These results suggested that dyes **1–3** of blue shift was occurred from electronic interaction with TiO<sub>2</sub>.<sup>25</sup>

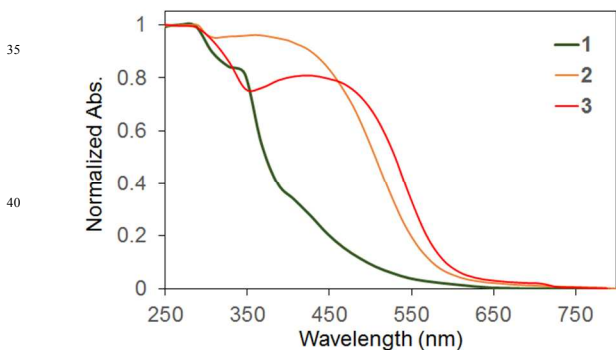


Figure 3. Absorption spectra of dyes **1–3** on TiO<sub>2</sub> films.

These absorption spectra suggested that the gaps between the highest occupied (HOMO) and the lowest unoccupied molecular orbitals (LUMO) of these dyes would become narrower as the number of spacers increased. To investigate the electronic properties, cyclic voltammetry was conducted in THF in the presence of Bu<sub>4</sub>NPF<sub>6</sub> (0.1 M) using Fc/Fc<sup>+</sup> as an internal standard (Fig. 4). Reversible one-electron oxidation potentials (*vs.* NHE) were observed at a  $E_{\text{ox}}^{1/2}(\text{I})$  value of +1.16 V for **1**, +1.07 V for **2** and +0.85 V for **3**. On the other hands, the reduction potentials of the LUMO levels of dye **1–3** could not estimate by cyclic voltammetry, due to one-electron irreversible reduction processes, i.e. the potentials (*vs.* NHE) found at a  $E_{\text{red}}^{\text{onset}}(\text{I})$  value of -1.33

V for **1**, -1.09 V for **2** and -1.07 V for **3** (Fig. S3). The LUMO levels of the sensitizers were estimated from their  $E_{\text{ox}}^{1/2}$  value and the edge of their absorption spectra. When the number of the spacers increased, the LUMO energies (*vs.* NHE) decreased in the order **1** (-1.18 V), **2** (-1.15 V) and **3** (-1.14 V). These potentials of trends were agreed with cyclic voltammetry results. All LUMO levels displayed high potentials compared to the conduction band of TiO<sub>2</sub> (-0.4 V *vs.* NHE), which is required to drive electron injection into TiO<sub>2</sub>. Furthermore, the reversible oxidations implied that the benzophenothiazine-containing dyes were highly stable during the oxidation–reduction process. These results suggest that dyes **1–3** may be suitable for photocatalytic reactions.

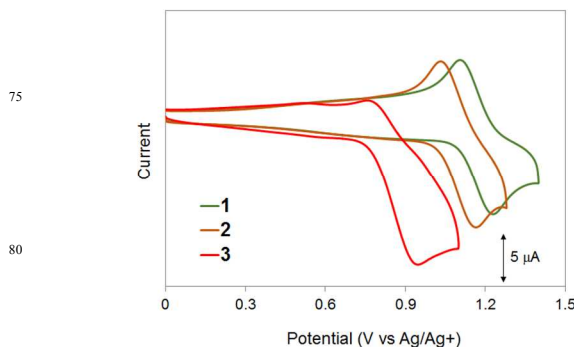


Figure 4. Cyclic voltammograms of **1–3** in 0.1 M Bu<sub>4</sub>NPF<sub>6</sub>-containing THF solutions. The scan rate was 100 mV/s.

### Theoretical Study

The donor–acceptor interactions of dyes **1–3** were further investigated through theoretical computations. Density functional theory (DFT) computations at the B3LYP/6-31G(d) level by Gaussian 09 program.<sup>26</sup> The result indicated that the cyano group of dye **1** must have a large dihedral angle (92°) with respect to the olefin bond to prevent steric effects between the olefin and the cyanoacrylic acid. On the other hand, the computational models showed much smaller dihedral angles for **2** (42°) and **3** (52°) because the insertion of the thiophene rings reduced the steric effects. Molecular orbitals (MOs) generated by DFT computations (B3LYP/6-31G(d) level) showed that the HOMO of **1** was located on the donor moiety but was not delocalized on the olefin bonds, indicating weak electronic interactions between the donor and olefin bonds and supporting the experimental results.

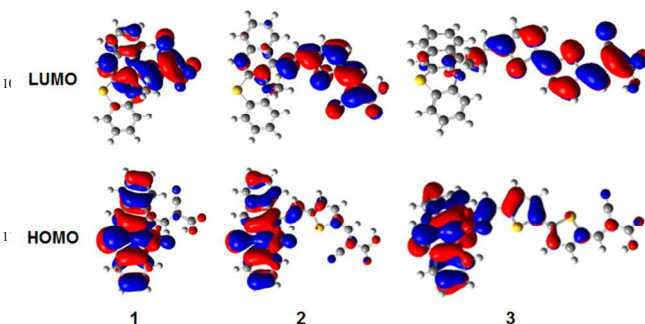


Figure 5. Generated molecular orbitals of HOMO and LUMO geometries from optimized structure of **1–3** at the B3LYP/6-31G(d) level.

5  
10 Table 1. Calculated (TDDFT/M06/6-31G(d)), experimental absorption (in THF and on TiO<sub>2</sub>), and electrochemical parameters for organic dyes.

Dyes	$\lambda_{\max}/f$ (nm/M <sup>-1</sup> cm <sup>-1</sup> ) <sup>a</sup>	$\lambda_{\max}/\epsilon$ (nm/M <sup>-1</sup> cm <sup>-1</sup> ) <sup>b</sup>	$\lambda_{\text{onset}}$ (nm) <sup>c</sup>	$\lambda_{\max, \text{TiO}_2}$ (nm)	$\Delta\lambda_{\max, \text{Soln.}-\text{TiO}_2}$ (nm)	HOMO/LUMO V vs NHE <sup>d</sup>	HOMO/LUMO (eV) <sup>e</sup>
<b>1</b>	388 (0.158)	363 (5122)	530	336	27	1.16/-1.18	-6.95/-1.81
<b>2</b>	446 (0.501)	391 (20312)	560	361	30	1.07/-1.15	-6.59/-2.28
<b>3</b>	451 (1.26)	443 (22239)	621	425	18	0.85/-1.14	-6.53/-2.36

<sup>a</sup> obtained by TDDFT at the M06/6-31G(d) level, *f*: oscillator strength for the lowest energy transition. <sup>b</sup>  $\epsilon$ : absorption coefficient. <sup>c</sup> measured in THF. <sup>d</sup> calibrated according to Fc/Fc<sup>+</sup> = -0.63 V vs. NHE. <sup>e</sup> obtained by TDDFT at the M06/6-31G(d) level.

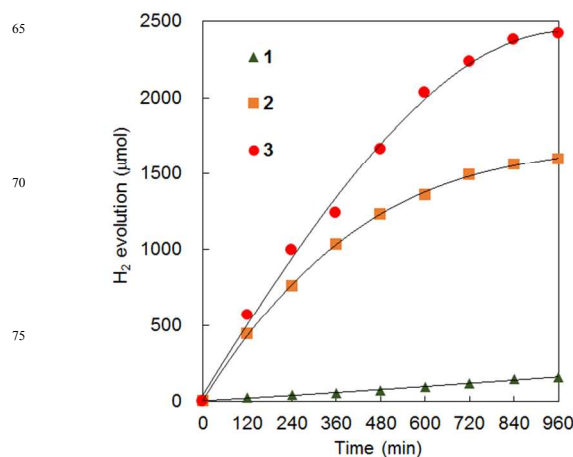
15 On the other hand, the HOMO levels showed good electronic coupling between the donor and spacer moieties for molecules **2** and **3**, consistent with efficient charge-transfer interactions between donor and acceptor (Fig. 5). Time-dependent (TD) DFT computations (M06/6-31Gd level) showed that trends observed in  
20 the computed HOMO–LUMO energy, lowest excitation energy and oscillator strengths for **1–3** were in good agreement with the experimental results. The physical properties of **1–3** are summarized in Table 1.

### 25 Water Splitting Reaction

To assess the performance of these dyes for photocatalytic water splitting reaction, the hydrogen production of TiO<sub>2</sub>/dye/Pt systems containing dyes **1–3** was investigated in 10% triethanolamine (TEA) of water (pH = 7). The TiO<sub>2</sub>/dye/Pt  
30 catalysts were fabricated on commercially available TiO<sub>2</sub> anatase particles by Pt photodeposition in methanol using a Xe lamp (300 W).<sup>27</sup> After this photodeposition, the dye was loaded onto the TiO<sub>2</sub>/Pt particles by solution processing in the presence of a 0.30 mM dye solution in methanol at room temperature for 12 h. The  
35 reflectance absorption spectra of the TiO<sub>2</sub> particles showed peaks at the same wavelengths as for dye–TiO<sub>2</sub> films (Fig. S1), confirming the appropriate loading of the dyes. The dye loading amounts on the TiO<sub>2</sub> catalyst were 0.65  $\mu\text{mol}/33 \text{ mg}$  for **1**, 0.91  $\mu\text{mol}/33 \text{ mg}$  for **2** and 0.96  $\mu\text{mol}/33 \text{ mg}$  for **3**. The low loading  
40 amount of dye **1** may be explained by its molecular structure. The N-methyl group of the donor moiety is very close to the cyanocarboxylic acid acceptor in **1**, reducing the ability of the dye to connect with the TiO<sub>2</sub> surface. On the other hand, in **2** and **3**, donor and acceptor moieties are separated by a bridge of  
45 thiophene spacers. Competition in the hydrogen production performances between dyes **2** and **3** is worth mentioning. After 16 h, dye **2** produced 1597  $\mu\text{mol}$  of hydrogen gas, whereas dye **3** produced 2141  $\mu\text{mol}$ . As a result, dye **3** exhibited higher turnover number (TON) and frequency (TOF) (TON = 4460; TOF = 278)  
50 than dye **2** (TON: 3510, TOF: 219) after 16 h. The hydrogen production performance of dye **1** was very low (TON: 483, TOF: 30) after 16 h (Fig. 6 and Table 2). One probable reason for the low production amount of hydrogen in dye **1** is its low loading amount on TiO<sub>2</sub> compared with those of the other dyes. Another  
55 reason may be the low excitation frequency and of dye **1** upon light stimulation over 420 nm. In solution, dye **1** displayed a low excitation coefficient (5122 nm/M<sup>-1</sup>cm<sup>-1</sup>) at its maximum

absorption peak ( $\lambda = 380 \text{ nm}$ ) and this coefficient became even weaker at 420 nm (3503 nm/M<sup>-1</sup>cm<sup>-1</sup>).

60 On the other hand, although dye **2** exhibited absorption maxima at 391 nm, dyes **2** and **3** both presented wide range and strong excitation coefficients above 420 nm (**2**: 16699 nm/M<sup>-1</sup>cm<sup>-1</sup>, **3**: 20167 nm/M<sup>-1</sup>cm<sup>-1</sup> at 420 nm).



80 Figure 6. Photocatalytic activities of dyes **1–3** in water splitting reactions. Reaction conditions: 10 vol% aqueous TEA (10 mL), 33.0 mg TiO<sub>2</sub>/dye/Pt catalyst, pH = 7.0.

The single component of wavelength at 420 nm was used to  
85 determine the quantum efficiency for hydrogen conversion of water (Fig. S4 and table S1). We estimated the efficiency at 420 nm (7.36 mW/cm<sup>2</sup>) was 1.65% for **3**, 1.46% for **2**, and very small yield of 0.03% for **1** was found, respectively. Even the effects of absorption range and excitation coefficient are considered by  
90 TON and quantum yield, hydrogen production rate at **1** is quite smaller than that of others. The difference of quantum efficiency at single wavelength suggested that the other factor should dominate for the rate of hydrogen production.

### 95 Time-resolved absorption spectra and theoretical studies of dyes on TiO<sub>2</sub>

A protecting group such as a long alkyl chain may enhance dye stability and performance in solar cell systems.<sup>18,21</sup> All model dyes are on a TiO<sub>2</sub> surface, i.e. benzophenothiazine donors  
100 without any bulky substituents, which may lead to the dyes

having similar stability in the hydrogen production process. However, dyes **2** and **3** exhibited a higher TON than dye **1**. Time-resolved absorption spectra were measured for dyes **1–3** on TiO<sub>2</sub> to investigate differe-

10

5

Table 2 Photocatalytic performance and the decay lifetimes of dyes **1–3** on TiO<sub>2</sub><sup>a</sup>.

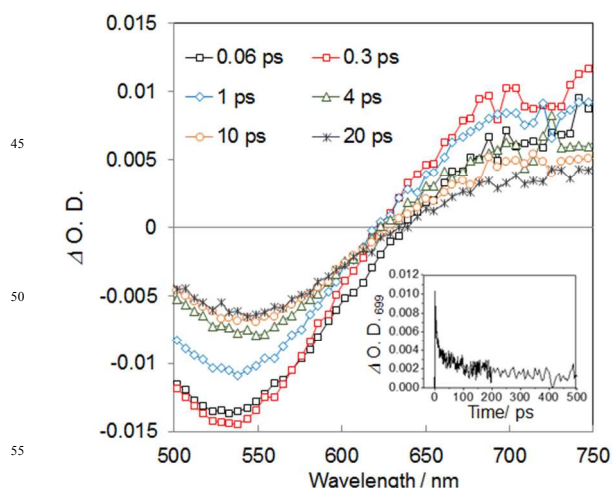
Dye	Dye loading amount (μmol/33mg)	Amount of H <sub>2</sub> (μmol) <sup>b</sup>	TON <sup>c</sup>	TOF <sup>d</sup>	Φ <sup>e</sup> (%)	τ <sub>1</sub> (ps)	τ <sub>2</sub> (ps)	τ <sub>3</sub> (ps)
<b>1</b>	0.65	157	483	30	0.03	0.17 <sup>f</sup>	- <sup>g</sup>	- <sup>g</sup>
<b>2</b>	0.91	1597	3510	219	1.46	0.31	3.64	47.0
<b>3</b>	0.96	2141	4460	278	1.65	0.60	7.00	85.4

<sup>a</sup> A 300 W Xe lamp was used and wavelengths below 420 nm were cut off using an optical filter. <sup>b</sup> H<sub>2</sub> produced after 16 h. <sup>c</sup> TON = (2 × amount of H<sub>2</sub> / dye loading amount after 16 h) / amount of dye. <sup>d</sup> Values after 16 h. <sup>e</sup> 420 nm (7.36 mW/cm<sup>2</sup>) of single wavelength was used. <sup>f</sup> *t* < ca. 5 ps was used to evaluate. <sup>g</sup> Not determined and single exponential decay fitting used because of the short decay profile of **1** at *t* > 5 ps

20

nances in their stabilities. Figure 7 shows typical spectra obtained for dye **3** on TiO<sub>2</sub>. In dye **3** solutions, a broadband radical cation with a maximum at 630 nm appeared within a few picoseconds (Fig. S5). This change in structural behaviour may result from vibrational relaxation and solvent reorganization. The time-resolved absorption spectra of **3** on TiO<sub>2</sub> film showed positive absorption above 620 nm for the radical cation species of **3** and a negative absorption difference below 620 nm induced by ground-state bleach.<sup>28</sup> The decay profiles monitored at 699 nm showed multi component decay up to after 300 ps, including shorter components (< ca. 5 ps) and longer component (> ca. 5 ps). The decay could be conveniently fitted with triple exponential decay functions for **2** and **3**, while single exponential decay function for **1**. The time decay constants of **3** were evaluated as τ<sub>1</sub> (0.60 ps), τ<sub>2</sub> (7.00 ps), and τ<sub>3</sub> (85.4 ps). Similar experiments for dye **2** gave time constants of τ<sub>1</sub> (0.31 ps) τ<sub>2</sub> (3.64 ps), and τ<sub>3</sub> (47.0 ps) (Figure 8, and Figs. S6 and S7). Dye **1** only presented one time constant over ca. 5 ps was found (Fig. 8a, and Figs. S6 and S7).

40



50

55

Figure 7. Time-resolved absorption spectra of dye **3** at 0.6–20 ps. Inset: Time-decay profiles of **3** at 699 nm.

60

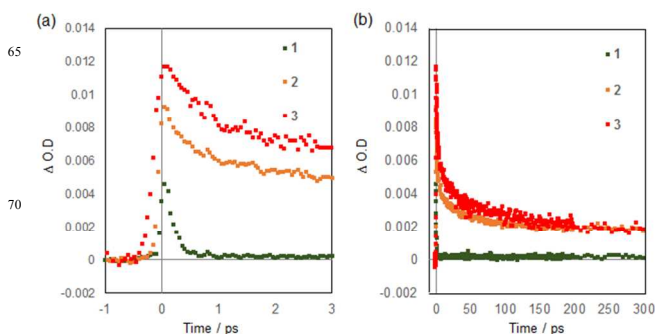


Figure 8. The kinetic decay profiles of dyes **1–3** on TiO<sub>2</sub>. (a): -1 to 3 ps range. (b): -10 to 300 ps range.

In the dye-loaded TiO<sub>2</sub> system, the multi-component decay occurs in the transient have been reported, due to various charge recombination processes were occurred between oxidised dye and in conduction band or trap site on TiO<sub>2</sub> surface.<sup>29</sup> The electron injection into TiO<sub>2</sub> is started ~100 fs scale at tarp sites of TiO<sub>2</sub>, and electron injection into TiO<sub>2</sub> at the conduction bands and/or trapping into the TiO<sub>2</sub> site are occurred over 100 ps.<sup>30</sup> Han *et al.* suggested that the decay component within < ca. 5 ps is charge recombination process between radical anion of TiO<sub>2</sub><sup>-</sup> at surface and/or shallow trap state and radical cation of dye<sup>+</sup>, while a component > ca. 5 ps can be injected the electron into the TiO<sub>2</sub> of conduction bands and/or trapping site. In the components of slower decay should play an important process to reduce the water to hydrogen, because of this major component may have the longer life time electrons at TiO<sub>2</sub> site.<sup>18</sup> The dye **1** showed shorter decay charge recombination component of τ<sub>1</sub> (0.18 ps) only, and could not find longer decay

component of  $\tau_2$ ,  $\tau_3$ . On the other hands, the dye **2** and **3** showed both shorter ( $\tau_1$ ) and longer ( $\tau_2$  and  $\tau_3$ ) components. In the dye **3** of major component  $\tau_3$  (85.4 ps) is longer than that of dye **2** (47.0 ps). Clearly, the time profiles of dyes **1–3** indicate that the lifetime of both radical cation species ( $\tau_1$  for **1**,  $\tau_1$ ,  $\tau_2$ , and  $\tau_3$  for **2** and **3**) increased when the number of spacers between donor and acceptor increased. This fact suggests that the spacer effect extended the charge recombination lifetimes between dye and  $\text{TiO}_2$ , because the separation provided by the thiophene ring spacers enhanced the time taken by the  $\text{TiO}_2$  electron to return to the dye or donor site. Therefore the dye **1** showed small TON and quantum efficiency. The longer decay component ( $\tau_3$ ) in **2** and **3** can provide the long-lived electron in  $\text{TiO}_2$ , thus the rate of hydrogen production can be improved.

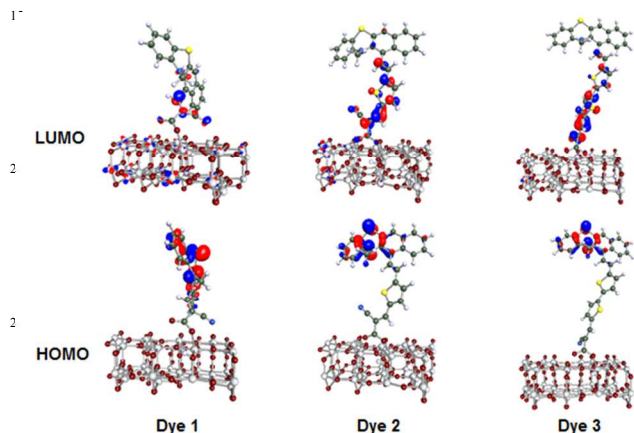


Figure 9. DFT/BP86 HOMO and LUMO geometries of optimized structures of dyes **1–3**@( $\text{TiO}_2$ )<sub>82</sub>

To estimate the coordination structure of dyes on  $\text{TiO}_2$ , calculations were performed with DFT/BP86 functional for  $\text{TiO}_2$  cluster and dye-molecules adsorbed on its surface.<sup>31,32</sup> The coordinates of the  $\text{TiO}_2$  atoms were kept fixed, while the coordinates of the dyes were fully relaxed. The calculations were performed with the DFT/BP86 functional and def-sv(p) basis set implemented in the Turbomole program.<sup>33</sup> Owing to the large size of the models calculations with hybrid DFT functional could not be applied. The Dyes **2** and **3** showed biadentate with carboxylate type coordination structure on  $\text{TiO}_2$ , because of the both carboxylate distances to  $\text{TiO}_2$  are almost same (2.1~2.3 Å for **2**@ $\text{TiO}_2$ , and 2.1~2.4 Å for **3**@ $\text{TiO}_2$  in Fig. 9 and Fig. S8). In this geometry, the dye molecules stand on the semiconductor surface, leading to a good separation between benzo[*b*]phenothiazine donor moieties and semiconductor. On the other hand, dye **1** displayed a monodentate with carboxylate type coordination (3.3 Å and 2.2 Å for Dye1@ $\text{TiO}_2$  in Fig. 9 and Fig. S8). We already discussed that the dye-loading amount of dye **1** (0.65  $\mu\text{mol}$ ) was much smaller than others cases (0.91  $\mu\text{mol}$  for **2** and 0.96  $\mu\text{mol}$  for **3**, in table 2), suggested difficulty of the dye **1** of carboxylate coordination on  $\text{TiO}_2$  surface. Coordination of different of dye **1**

probably came from to avoid a repulsive steric effect toward  $\text{TiO}_2$  surface due to the rotation of the donor site itself and/or the N-methyl group of the donor moiety. In this structure, the dye molecule lies on the semiconductor surface, resulting in a short distance between donor moiety and semiconductor. The molecular orbital of HOMOs of dye **1–3**@ ( $\text{TiO}_2$ )<sub>82</sub> and LUMOs of dye **2–3**@ ( $\text{TiO}_2$ )<sub>82</sub> were similar to their corresponding HOMO and LUMO geometries obtained without  $\text{TiO}_2$  (Fig. 5). However, the LUMO of dye **1**@ ( $\text{TiO}_2$ )<sub>82</sub> showed that most molecular orbitals did not cover the dye but were delocalized on the semiconductor. This result suggested that many electrons were trapped in the  $\text{TiO}_2$  surface via through-space electron injection from the donor because of the close proximity between the dye and the semiconductor surface. As a result, efficient charge injection into  $\text{TiO}_2$  by the spacer effects can reduce the number of times the charge recombination to the ground state without the excited dyes conducting charge injection into  $\text{TiO}_2$ . Thus, the biadentate with carboxylate type coordination structure of dyes **2** and **3** of the TON were enhanced. Dye **1** exhibited a small TON and its  $\tau_2$  and  $\tau_3$  value was not evaluated because of its fast decay. This may be explained by the difference of monodentate coordination with other dyes **2** and **3**, and/or short coordination distance between the donor and  $\text{TiO}_2$ , which allowed the charge recombination to occur without an effective charge injection into  $\text{TiO}_2$ .

## Conclusion

In conclusion, novel donor–spacer–acceptor dyads containing benzo[*b*]phenothiazine as the donor unit were synthesized. Thiophenes attached at the 10-position of the benzo[*b*]phenothiazine reduced the dihedral angle between donor and acceptor, readily increasing the charge-transfer electronic coupling between these units. The benzo[*b*]phenothiazine-containing dyes exhibited good donating ability and stability and their physical properties could be explained by DFT computations. Dyes **1–3** were incorporated in  $\text{TiO}_2$ /dye/Pt catalysts and the visible-light-driven photocatalytic hydrogen production of these catalysts was assessed at pH 7 in 10% aqueous TEA. The highest hydrogen production was observed for **3**, which showed hydrogen production rate of 4460 TON and 278 TOF after 16 h, with 1.65 % at 420 nm of quantum efficiency for hydrogen conversion of water. Time-resolved absorption spectra of the dye **1** displayed single-decay component of a short cation radical decay, while the dyes **2** and **3** on  $\text{TiO}_2$  showed multi-decay components that presented longer decays when the number of spacers increased. The computation results dye **1–3**@ ( $\text{TiO}_2$ )<sub>82</sub> with the DFT/BP86 functional and def-sv(p) basis set suggested that the dyes **2** and **3** showed standing geometry on  $\text{TiO}_2$  with bidentate structure, while lying geometry on  $\text{TiO}_2$  due to monodentate structure. In our water splitting reaction and time-resolved results combined with theoretical computation suggested that the spacer can be reduced the charge combination from  $\text{TiO}_2$  and enhanced charge injection into  $\text{TiO}_2$ , and making a bidentate

binding mode due to reduce the steric effect between the donor moiety and TiO<sub>2</sub> site. Dye **3** showed superior hydrogen production performance, which showed great value as a metal-free organic dye for water splitting cell in TiO<sub>2</sub>/dye/ Pt system. Further studies of new dyads are currently underway to improve dye stability for visible-light-driven photocatalytic hydrogen production in aqueous media.

## Acknowledgements

This work was supported by World Premier International Research Center Initiative (WPI), and a Grant-in-Aid for Science Research (26810107) from Ministry of Education, Culture, Sports, Science and Technology of Japan (MEXT), Japan. The computations (Gaussian 09 program) were carried out by using the computer facilities at the Research Institute for Information Technology, Kyushu University.

## Notes and references

- a) A. J. Bard and M. A. Fox, *Acc. Chem. Res.*, 1995, **28**, 141.; b) H. Arakawa, M. Aresta, J. N. Armor, M. K. Barteau, E. J. Beckmen, A. T. Bell, J. E. Bercaw, C. Creutz, E. Dinjus, D. A. Dixon, K. Doumen, D. L. DuBois, J. Eckert, E. Fujita, D. H. Gibson, W. A. Goddard, D. W. Goodman, J. Keller, G. J. Kubas, H. H. Kung, J. E. Lyons, L. E. Manzer, T. J. Marks, K. Morokuma, K. M. Nicholas, R. Periana, L. Que, J. Rostrop-Nielsen, W. M. H. Sachtler, L. D. Schmidt, A. Sen, G. A. Somorjai, P. C. Stair, B. R. Stults and W. Tumas, *Chem. Rev.*, 2001, **101**, 953.; c) C. Song, *Cat. Today*, 2006, **115**, 2.; d) T. E. Mallouk, *Nat. Chem.*, 2013, **5**, 362.
- A. Fujishima and K. Honda, *Nature*, 1972, **238**, 37.
- K. Hashimoto, H. Irie and A. Fujishima, *J. J. Appl. Phys.* 2005, **44**, 8269.
- M. Ni, M. K.H. Leung, D. Y. C. Leung and K. Sumathy, *Ren. Sus. Energy Rev.*, 2007, **11**, 401.
- A. Kudo and Y. Miseki, *Chem. Soc. Rev.*, 2009, **38**, 253.
- M. G. Walter, E. L. Warren, J. R. Mckone, S. W. Boettcher, Q. M. Ei, E. A. Santori, and N. S. Lewis, *Chem. Rev.*, 2010, **110**, 6446.
- R. M. N. Yerga, M. C. Álvarez-Galván, F. del Valle, J. A. V. de la Mano and J. L. G. Foerro, *Chem. Sus. Chem.*, 2009, **2**, 471.
- R. M. Navrro, F. del Valle, J. A. V. de la Mano, M. C. Álvarez-Galvan, and J. L. G. Fierro, *Adv. Chem. Engineer.*, 2009, **36**, 111.
- M. Grätzel, *Chem. Lett.*, 2005, **34**, 8.
- a) W. J. Youngblood, S.-Y. A. Lee, K. Maeda and T. M. Mallouk, *Acc. Chem. Res.*, 2009, **42**, 1966. b) J. R. Swierk and T. E. Mallouk, *Chem. Soc. Rev.*, 2013, **42**, 2357.
- a) E. Borgarello, J. Kiwi, E. Perlizetti, M. Visca and M. Grätzel, *Nature*, 1981, **289**, 158.; b) T. Kajiwara, K. Hashimoto, T. Kawai and T. Sakata, *J. Phys. Chem.*, 1982, **88**, 4516.; c) Y. I. Kim, S. J. Atherton, E. S. Brigham and T. E. Mallouk, *J. Phys. Chem.* 1993, **97**, 11802.; d) K. Hirano, E. Suzuki, A. Ishikawa, T. Moroi, H. Shiroishi and M. Kaneko, *J. Photochem. Photobio. A.*, 2000, **136**, 157.; e) K. Maeda, M. Eguchi, W. J. Youngblood and T. E. Mallouk, *Chem. Mater.* 2008, **20**, 6770.; f) X. Zhang, U. Veikko, J. Mao, P. Cai and T. Peng, *Chem. Eur. J.*, 2012, **18**, 12103.; g) H. Luo, W. Song, P. G. Hoertz, K. Hanson, R. Ghosh, S. Rangan, M. K. Brennaman, J. J. Concepcion, R. A. Binstear, R. A. Bartynski, R. Lopez and T. J. Mayer, *Chem. Mater.*, 2013, **25**, 122.
- a) E. A. Malinka, G. L. Kamalov, S. V. Vodziskii, V. I. Melnik and Z. I. Zhilina, *J. Photochem. Photobio. A.*, 1995, **90**, 153.; b) K. Takanabe, K. Kamata, X. Wang, M. Antonietti, J. Kubota and K. Domen, *Phys. Chem. Chem. Phys.*, 2010, **12**, 13020.; c) W. Kim, T. Tachikawa, T. Majima, C. Li, H.-J. Kim and W. Choi, *Energy Environ. Sci.*, 2010, **3**, 1789.
- a) R. Abe, K. Sayama and H. Arakawa, *J. Photochem. Photobio. A.*, 2004, **166**, 115.; b) R. Abe, K. Shinmei, K. Hara and B. Ohtani, *Chem. Commun.*, 2009, 3577.
- S. Y. Kuchirni, A. V. Korzhak, N. F. Guba, S. V. Kulik and A. I. Kryukov, *Theor. Exper. Chem.*, 1995, **31**, 309.
- a) T. Shimizu, T. Iyoda and Y. Koide, *J. Am. Chem. Soc.*, 1985, **107**, 35.; b) X. Zhang, Z. Jin, Y. Ki, S. Li and G. Lu, *J. Phys. Chem. C* 2009, **113**, 2630.; c) P. Chowdhury, H. Goma and A. K. Ray, *Int. J. Hydro. Energy*, 2011, **36**, 13442.
- F.-S. Liu, R. Ji, Min, Wu and Y.-M. Sun, *Acta Phys. Chim. Sin.*, 2007, **23**, 1899.
- S. Ikeda, C. Abe, T. Torimoto and B. Ohtani, *J. Photochem. Photobio. A.*, 2003, **160**, 61.
- W.-S. Han, K.-R. Wee, H.-Y. Kim, C. Pac, Y. Nabetani, D. Yamamoto, T. Shimada, H. Inoue, H. Choi, K. Cho and S. O. Kang, *Chem. Chem. Eur. J.* 2012, **18**, 15368
- J. Lee, J. Kwak, K. C. Ko, J. H. Park, J. H. Ko, N. Park, E. Kim, D. H. Ryu, T. K. Ahn, Y. J. Lee and S. U. Son, *Chem. Commun.*, 2012, **48**, 11431.
- a) S. Hwang, J. H. Lee, C. Park, H. Lee, C. Kim, C. Park, M.-H. Lee, W. Lee, J. Park, K. Kim, N.-G. Park and C. Kim, *Chem. Commun.* 2007, 4887. b) S. Ito, H. Miura, S. Uchida, M. Takata, K. Sumioka, P. Liska, P. Comte, P. Pechy and M. Grätzel, *Chem. Commun.* 2008, 5194. c) Y. J. Chang and T. J. Chow, *Tetrahedron*, 2009, **65**, 4726.
- Y. J. Chang, M. Watanabe, P.-T. Chou and T. J. Chow, *Chem. Commun.*, 2012, **48**, 726.
- A. Mishra, M. K. R. Fischer and P. Bäuerle, *Angew. Chem. Int. Ed.*, 2009, **48**, 2474.
- a) Q. Wang, W. M. Campbell, E. E. Bonfantani, K. W. Jolley, D. L. Officer, P. J. Walsh, K. Gordon, R. Humphry-Baker, M. K. Nazeeruddin and M. Grazel, *J. Phys. Chem. B.* 2005, **109**, 15397.; b) J.-J. Cid, J.-J. Yum, S.-R. Jang, M. K. Nazeeruddin, E. Martínez-Ferrero, E. Palomares, J. Ko, M. Grätzel and T. Torres, *Angew. Chem. Int. Ed.* 2007, **46**, 8358.; c) T. Besso, S. M. Zakeeruddin, C.-Y. Yeh, E. W.-G. Diau and M. Grätzel, *Angew. Chem. Int. Ed.* 2010, **49**, 6646.
- a) H. Tian, X. Yang, R. Chen, Y. Pan, L. Li, A. Hagfeldt and L. Sun, *Chem. Commun.*, 2007, 3741.; (b) S. H. Kim, H. W. Kim, C. Sakong, J. Namgoong, S. W. Park, M. J. Ko, C. H. Lee, W. I. Lee and J. P. Kim, *Org. Lett.*, 2011, **13**, 5784.; (c) W. Wu, J. Yang, J. Hua, J. Tang, L. Zhang, Y. Long and H. Tian, *J. Mater. Chem.*, 2010, **20**, 1722.; (d) M. Marszalek, S. Nagane, A. Ichake, R. Humphry-Baker, V. Paul, S. M. Zakeeruddin and M. Grätzel, *J. Mater. Chem.*, 2012, **22**, 889.; (e) C. Chen, J.-Y. Liao, Z. Chi, B. Xu, X. Zhang, D.-B. Kuang, Y. Zhang, S. Liu and J. Xu, *J. Mater. Chem.*, 2012, **22**, 8994.; (f) T. Meyer, D. Ogermann, A. Pankrath, K. Kleinermanns and T. J. J. M. F. uller, *J. Org. Chem.*, 2012, **77**, 3704. g) Y. J. Chang, P.-T. Chou, Y.-Z. Lin, M. Watanabe, C.-J. Yang, T.-M. Chin and T. J. Chow, *J. Mater. Chem.*, 2012, **22**, 21704. h) A. S. Hart, C. Bikram K. C., N. K. Subbaiyan, P. A. Karr and F. D'Souza, *ACS Appl. Mater. Interfaces*, 2012, **4**, 5813.
- D. P. Hagberg, T. Edvinsson, T. Marinado, G. Boschloo, A. Hagfeldt, L. Sun, *Chem. Commun.*, 2006, 2245.
- M. J. Frisch, G. W. Trucks, H. B. Schlegel, G. E. Scuseria, M. A. Robb, J. R. Cheeseman, G. Scalmani, V. Barone, B. Mennucci, G. A. Petersson, H. Nakatsuji, M. Caricato, X. Li, H. P. Hratchian, A. F. Izmaylov, J. Bloino, G. Zheng, J. L. Sonnenberg, M. Hada, M. Ehara, K. Toyota, R. Fukuda, J. Hasegawa, M. Ishida, T. Nakajima, Y. Honda, O. Kitao, H. Nakai, T. Vreven, J. A. Montgomery, Jr., J. E. Peralta, F. Ogliaro, M. Bearpark, J. J. Heyd, E. Brothers, K. N. Kudin, V. N. Staroverov, T. Keith, R. Kobayashi, J. Normand, K. Raghavachari, A. Rendell, J. C. Burant, S. S. Iyengar, J. Tomasi, M. Cossi, N. Rega, J. M. Millam, M. Klene, J. E. Knox, J. B. Cross, V. Bakken, C. Adamo, J. Jaramillo, R. Gomperts, R. E. Stratmann, O. Yazyev, A. J. Austin, R. Cammi, C. Pomelli, J. W. Ochterski, R. L. Martin, K. Morokuma, V. G. Zakrzewski, G. A. Voth, P. Salvador, J. J. Dannenberg, S. Dapprich, A. D. Daniels, O. Farkas, J. B. Foresman, J. V. Ortiz, J. Cioslowski, D. J. in Gaussian 09, Revision C.01, Gaussian, Inc., Wallingford CT, 2010.
- J.-M. Herrmann, J. Disdier and P. Pichat, *J. Phys. Chem.*, 1986, **90**, 6028.
- R. Bererem R. V. Grondelle, J. T. M. Kennis, *Photosynth Res.* 2009, **101**, 105.

- 29 J. R. Drrant, S. A. Haque, E. Palomares, *Coord. Cgem. Rev.*, 2004, 248, 1257-1257.
- 30 a) S. H. Szczepankiewicz, J. A. Moss and M. R. Hoffmann, *J. Phys. Chem. B*, 2002, **106**, 2922. b) J. Kallioinen, V. Lehtovuori, P. Myllyperio, J. Korppi-Tommola, *Chem. Phys. Lett.* 2001, **340**, 217.
- 5 c) J. Wiberg, T. Marinado, D. P. Hagberg, L. Sun, A. Hagfeldt, B. Albinsson, *J. Phys. Chem. C*. 2009, **113**, 83881. d) S. Kaniyankandy, S. Verma, J. A. Mondal, D. K. Palit, H. N. Ghosh, *J. Phys. Chem. C*. 2009, **113**, 3593.
- 10 31 F. Nunzi, E. Mosconi, L. Storch, E. Ronca, A. Selloni, M. Grätzel, F. De Angelis, *Energy Environ. Sci.* **2013**, *6*, 1221.
- 32 I. Bandyopadhyay, C. M. Aikens, *J. Phys. Chem. A* **2011**, *115*, 868.
- 33 R.. Ahlrichs, M. Bar, M. Haser, H. Horn, C. Kolmel, *Chem. Phys. Lett.* 1989, **162**, 165.

## 15 Experimental Section

### General Information

The  $^1\text{H}$  and  $^{13}\text{C}$  NMR were recorded on a BrukerAV500 (500 MHz) and AV500 (400 MHz). The  $^1\text{H}$  and  $^{13}\text{C}$  NMR chemical shifts were reported as  $\delta$  values (ppm) relative to external  $\text{Me}_4\text{Si}$ . The coupling constants ( $J$ ) were given in hertz. MALDI mass spectra were recorded on a Bruker Autoflex. The sample was dissolved in dichloromethane first, then an equal amount of this sample solution (1.0  $\mu\text{L}$ ) and a dithranol in dichloromethane (DIT, 1.0  $\mu\text{L}$ ) was spotted onto the stainless steel sample plate for injection together. High resolution mass spectra were recorded on a JEOL LMS-HX-110 spectrometer. FAB MS spectra were measured with 3-nitrobenzyl alcohol (NBA) as the matrix. Analytical thin layer chromatography (TLC) was performed on silica gel 60 F<sub>254</sub> Merck. Column chromatography was performed on KANTOSI60N (neutral). Absorption spectra were recorded on a SIMAZU IR spectrophotometer. IR spectra were recorded on a SHIMAZU spectrometer. Redox potentials were carried out on a BAS-100B/W electrochemical analyzer. CV measurements were performed using a cell equipped with glassy carbon as the working electrode, platinum wire as the counter electrode, and Ag/AgNO<sub>3</sub> as the reference electrode. All electrochemical measurements were performed under an Ar atmosphere at room temperature in THF solution ( $5 \times 10^{-4}$  M) containing 0.10 M tetra-n-butylammoniumhexafluorophosphate ( $\text{Bu}_4\text{NPF}_6$ ) as a supporting electrolyte at a scan rate of 100 mV/s. The ferrocene/ferrocenium ( $\text{Fc}/\text{Fc}^+$ ) couple was used as an internal standard. THF was distilled from sodium benzophenone ketyl. Toluene was distilled from  $\text{CaH}_2$ . Other solvents and reagents were of reagent quality, purchased commercially, and used without further purification.

### Dye-loaded 1.0 wt% Pt-TiO<sub>2</sub> nanoparticle

The procedure of 1.0 wt% Pt-loaded TiO<sub>2</sub> nanoparticle was followed repeatedly.<sup>25</sup> The commercially available of TiO<sub>2</sub> source (1.0 g, < 25 nm, anatase) was added MeOH (25 mL) and H<sub>2</sub>PtCl<sub>6</sub> (0.25 mL, 8wt%). The mixture was irradiated the Xe lamp (300 W) at 25 min., produced TiO<sub>2</sub>-Pt nanoparticle. The TiO<sub>2</sub>-Pt nanoparticle was separated by centrifuge (3600 rpm 20 min), then separated TiO<sub>2</sub>-Pt nanoparticle was filtrated, washed MeOH successively. This was dried under vacuum, gave Pt-loaded TiO<sub>2</sub> nanoparticle.

1.0 wt% Pt-loaded TiO<sub>2</sub> (100 mg) was immersed in a MeOH solution containing  $3 \times 10^{-4}$  M dye sensitizers (10 mL) for at least 12 h under the dark, centrifuged (3600 rpm 20 min), rinsed with anhydrous MeOH and dried under vacuum.

### Water splitting reaction

The photocatalytic water splitting experiment was performed

with a conventional closed circulating system with a dead volume of approximately 500 ml. The Pt/dye/TiO<sub>2</sub> catalyst 33 mg was suspended in 10 ml of 10 v/v% triethanol amine water (pH= 7.0, adjust with HCl.aq). A quartz reaction cell was irradiated by an external light source comprising a 300 W Xe lamp (Ushio Inc., Japan) with < 420 nm cutoff glass filter. During the H<sub>2</sub>O photochemical reaction, reaction mixture was mixed with a magnetic stirring bar. Amounts of H<sub>2</sub> gas amount was measured with a TCD gas chromatograph (GC-8A, Shimadzu Corp., Japan, which was connected to a conventional volumetric circulating line with a vacuum pump.

To determine the quantum efficiency for hydrogen conversion of water. We estimated the efficiency by changing the light source equipment for using a single wavelength at 420 nm (7.36 mW/cm<sup>2</sup>) (ASAHI SPECTRA MAX-303). The reaction surface area were 17.34 cm<sup>2</sup>. The calculation of the quantum efficiency at 420±10 nm was used as equation 1.

$$\phi = \frac{\text{Number of electrons}}{\text{Number of incident photons}} \quad (1)$$

### 85 Time resolved absorption measurements

The titania-oxide pastes of Ti-nanoxide T/SP that was purchased from Solaronix. The quartz plate (transmission > 90% in the visible) was used as substrate. A thin film of TiO<sub>2</sub> (8–10 nm) was coated on a quartz substrate. It was immersed in an anhydrous MeOH solution containing  $3 \times 10^{-4}$  M dye sensitizers for at least 12 h, then rinsed with anhydrous MeOH and dried. Time resolved absorption spectra of dyes on thin-film or in solution were performed in an ambient atmosphere. The femtosecond time resolved absorption data were collected with a pump and probe time-resolved absorption spectroscopy system (Ultrafast Systems, Helios). The pump light (400 nm) was used from an amplified Ti-sapphire laser system (Spectra-Physics, Solstice-100F, < 100 fsec, 5 kHz). The UV/Vis range (450-750 nm) was detected with a linear CCD array (Ocean Optics, S2000). The fitting was used triple exponential decay fitting as equation 2 for dye 2 and 3, while single exponential decay fitting as equation 3 for dye 1.

$$\Delta OD = A_1 \exp\left[-\frac{(t-t_0)}{\tau_1}\right] + A_2 \exp\left[-\frac{(t-t_0)}{\tau_2}\right] + A_3 \exp\left[-\frac{(t-t_0)}{\tau_3}\right] + A_{off} \quad (2)$$

$$\Delta OD = A_1 \exp\left[-\frac{(t-t_0)}{\tau_1}\right] + A_{off} \quad (3)$$

110 ,where  $A_{off}$  is off-set of intensity at the fitting range of decay.

### Synthetic Procedure

#### 12-methyl-12H-benzo[b]phenothiazine 5

A Mixture of 12H-benzo[b]phenothiazine 4 (3.05 g, 12.2 mmol) and THF (100 mL) were added the tBuOK (2.06 g, 18.4 mmol) at 0 °C in N<sub>2</sub> atmosphere. After 30 min, MeI (1.53 mL, 24.6 mmol) was added one portion and the mixture was stirred overnight at room temperature in N<sub>2</sub> atmosphere. The mixture was quenched with water, extracted with CH<sub>2</sub>Cl<sub>2</sub>, washed by anhyd. MgSO<sub>4</sub>. Silicagel chromatography with CH<sub>2</sub>Cl<sub>2</sub>:hexane=1:3 to give 12-methyl-12H-benzo[b]phenothiazine 5 (1.42 g, 44 %) as pale yellow solid.

Physical data of 5: Mp184-186°C.  $\delta_{\text{H}}$  (CDCl<sub>3</sub>, 500 MHz) 3.49 (s, 3H), 6.88 (d, J = 6.6 Hz, 1H), 6.94-6.96 (m, 1H), 7.06 (s 1H),

7.18-7.21 (m, 2H), 7.26-7.29 (m, 1H), 7.34-7.37 (m, 1H), 7.59 (s, 1H), 7.62 (d, J = 8.1 Hz, 1H), 7.67 (d, J = 7.1 Hz, 1H).  $\delta_{\text{C}}$  (CDCl<sub>3</sub>, 125 MHz) 35.7, 109.6, 114.6, 122.2, 123.0, 124.2, 125.0, 125.6, 126.0, 126.5, 126.8, 127.0, 127.4, 130.0, 133.4, 143.6, 144.9. MS (MALDI)  $m/z$  [M+H]<sup>+</sup>: calcd for C<sub>17</sub>H<sub>14</sub>NS:264, found: 264.

12-methyl-12*H*-benzo[*b*]phenothiazine-11-carbaldehyde **6**  
A Mixture of DMF (20 mL) and POCl<sub>3</sub> (16.54 mL, 1.54 mmol) was stirred at room temperature in N<sub>2</sub> atmosphere. After 1 h, benzo[*b*]phenothiazine **5** (1.32 g, 5.01 mmol) was added and heated at 60 °C for 36 h. The reaction mixture was poured into iced-water, extracted with CH<sub>2</sub>Cl<sub>2</sub>. Organic layer was washed with water, and dried with anhyd MgSO<sub>4</sub>. Silicagel chromatography with CH<sub>2</sub>Cl<sub>2</sub>:hexane=1:1 to give 12-methyl-12*H*-benzo[*b*]phenothiazine-11-carbaldehyde **6** (1.14 g, 78 %) as pale yellow solid.

Physical data of **6**: Mp104-105°C.  $\delta_{\text{H}}$  (CDCl<sub>3</sub>, 500 MHz) 3.74 (s, 3H), 7.01-7.05 (m, 1H), 7.11-7.16 (m, 2H), 7.22-7.26 (m, 1H), 7.36-7.39 (m, 1H), 7.48-7.52 (m, 1H), 7.60 (d, J=7.95, 1H), 7.64 (s, 1H), 8.88 (d, J=4.6, 1H), 10.4 (s, 1H).  $\delta_{\text{C}}$  (CDCl<sub>3</sub>, 125 MHz) 47.0, 118.4, 119.3, 123.8, 124.4, 125.4, 125.5, 126.6, 127.0, 127.5, 128.3, 129.5, 130.2, 130.9, 131.0, 145.6, 150.4, 190.4. ; MS (MALDI)  $m/z$  [M+H]<sup>+</sup>: calcd for C<sub>18</sub>H<sub>14</sub>NOS; 292, found: 292.

11-(bromotriphenylphosphoranyl)-12-methyl-12*H*-benzo[*b*]phenothiazine **8**

The mixture of aldehyde **6** (1.28 g, 4.39 mmol) and dried THF (60 mL) was added NaBH<sub>4</sub> (373 mg, 9.80 mmol) at 0 °C in N<sub>2</sub> atmosphere. After 3h, the mixture was quenched with water, extracted with CH<sub>2</sub>Cl<sub>2</sub>. Organic layer was washed with brine, and dried with anhyd Na<sub>2</sub>SO<sub>4</sub>. Removal the solvent gave diol **7** (1.24 g). This crude compound was used in the next step without further purification.

To the mixture of diol **7** (1.24 g, 4.22 mmol), PPh<sub>3</sub>HBr (1.45 g, 4.22 mmol), and dried toluene (50 mL) was refluxed for 1h in N<sub>2</sub> atmosphere. The mixture was dried, then washed by cooled toluene to give adduct **8** as light yellow powder (2.30 g, two steps, 88 %).

Physical data of **8**: yellow powder (EtOH). Mp173-175°C.  $\delta_{\text{H}}$  (CDCl<sub>3</sub>, 500 MHz) 3.38 (s, 3H), 5.36 (bs, 1H), 6.35 (bs, 1H), 6.49 (t, J = 3.7 Hz, 1H), 6.95 (t, J = 4.1 Hz, 2H), 7.03 (t, J = 5.9 Hz, 2H), 7.24 (t, J = 7.2 Hz, 1H), 7.40-7.48 (m, 12H), 7.54-7.58 (m, 5H), 7.88 (d, J = 8.3 Hz, 1H).  $\delta_{\text{C}}$  (CDCl<sub>3</sub>, 100 MHz) 26.1, 26.5, 46.8, 117.6, 118.3, 118.6, 118.7, 124.4, 124.9, 125.4, 125.5, 125.56, 125.6, 126.3, 126.37, 126.4, 127.0, 127.2, 127.3, 128.2, 129.9, 130.0, 131.56, 131.6, 131.8, 132.16, 132.2, 134.0, 134.1, 134.55, 134.6, 144.5, 144.6, 146.1.; MS (MALDI)  $m/z$  [M-Br+H]<sup>+</sup>: calcd for C<sub>36</sub>H<sub>30</sub>NPS539; found: 539.

(*E*)-2-cyano-3-(12-methyl-12*H*-benzo[*b*]phenothiazin-11-yl)acrylic acid **9**

The mixture of thiophene-2,5-dicarboxyaldehyde **9** (1.18 g, 8.42 mmol), 18-crown-6 (30 mg, 0.11 mmol), K<sub>2</sub>CO<sub>3</sub> (570 mg, 4.12 mmol), and DMF (30 mL) was dropwised the mixture of adduct **8** (1.30 g, 2.10 mmol) in DMF (30 mL) over 3h at 70 °C in N<sub>2</sub> atmosphere. The reaction mixture was stirred further 3h at 70 °C. The reaction mixture was quenched with water, extracted with CH<sub>2</sub>Cl<sub>2</sub>. The organic layer was washed with brine, dried with anhyd MgSO<sub>4</sub>. Silicagel chromatography with

CH<sub>2</sub>Cl<sub>2</sub>:hexane=1:5-1:1 to give aldehyde **10** (442 mg, 56%).

Physical data of **9**: Mp130-132°C.  $\delta_{\text{H}}$  (CDCl<sub>3</sub>, 500 MHz) 3.43 (s, 3H), 6.77 (d, J = 16.3 Hz, 1H), 6.93 (d, J = 10.0 Hz, 1H), 6.98 (t, J = 7.4 Hz, 1H), 7.15-7.23 (m, 3H), 7.33-7.40 (m, 2H), 7.55 (s, 1H), 7.62-7.66(m, 2H), 7.71 (d, J = 3.8 Hz, 1H), 7.95 (d, J = 8.4 Hz, 1H), 9.91 (s, 1H),  $\delta_{\text{C}}$  (CDCl<sub>3</sub>, 125 MHz) 43.4, 117.9, 121.5, 123.2, 123.6, 124.7, 125.0, 126.1, 126.3, 126.6, 126.62, 127.0, 127.2, 127.4, 129.4, 130.4, 131.8, 132.5, 137.1, 141.9, 142.2, 147.8, 152.0, 182.5.; MS (MALDI)  $m/z$  [M+H]<sup>+</sup>: calcd for C<sub>24</sub>H<sub>18</sub>NOS<sub>2</sub>400; found: 400.

(*E*)-5-(2-(12-methyl-12*H*-benzo[*b*]phenothiazin-11-yl)vinyl)thiophene-2-carbaldehyde **10**

The mixture of [2,2'-bithiophene]-5,5'-dicarbaldehyde **10** (444 mg, 2.00 mmol), 18-crown-6 (28 mg, 0.11 mmol), K<sub>2</sub>CO<sub>3</sub> (550 mg, 3.98 mmol), and DMF (30 mL) was dropwised the mixture of adduct **8** (1.24 g, 2.00 mmol) in DMF (30 mL) over 3h at 70 °C in N<sub>2</sub> atmosphere. The reaction mixture was stirred further 3h at 70 °C. The reaction mixture was quenched with water, extracted with CH<sub>2</sub>Cl<sub>2</sub>. The organic layer was washed with brine, dried with anhyd MgSO<sub>4</sub>. Silicagel chromatography with CH<sub>2</sub>Cl<sub>2</sub>:hexane=1:5-1:1 to give aldehyde **10** (484 mg, 50 %).

Physical data of **10**: Mp150-152°C.  $\delta_{\text{H}}$  (CDCl<sub>3</sub>, 500 MHz) 3.47 (s, 3H), 6.72 (d, J = 16.2 Hz, 1H), 6.93-6.99 (m, 2H), 7.18-7.24 (m, 2H), 7.32 (dd, J = 5.5, 3.9 Hz, 2H), 7.33-7.36 (m, 1H), 7.38-7.41 (m, 1H), 7.45 (d, J = 16.2 Hz, 1H), 7.56 (s, 1H), 7.64 (d, J = 7.9 Hz, 1H), 7.71 (d, J = 3.9 Hz, 1H), 7.99 (d, J = 8.3 Hz, 1H), 9.89 (s, 1H).  $\delta_{\text{C}}$  (CDCl<sub>3</sub>, 125 MHz) 43.3, 117.8, 122.0, 123.1, 123.8, 124.2, 124.3, 124.5, 126.0, 126.1, 126.3, 126.6, 126.8, 127.1, 127.3, 127.4, 127.41, 130.4, 131.8, 132.7, 134.5, 137.2, 141.6, 141.8, 144.4, 146.8, 148.0, 182.3.; MS (MALDI)  $m/z$  [M+H]<sup>+</sup>: calcd for C<sub>28</sub>H<sub>20</sub>NOS<sub>3</sub>482; found: 482.

(*E*)-2-cyano-3-(12-methyl-12*H*-benzo[*b*]phenothiazin-11-yl)acrylic acid **1**

A mixture of aldehyde **6** (633 mg, 1.58 mmol), cyanoacetic acid (820 mg, 9.64 mmol), ammonium acetate (36 mg, 0.45 mmol), and glacial acetic acid (70 mL) was heated at 90 °C for overnight in N<sub>2</sub> atmosphere. After reaction mixture was cooled, the reaction was quenched with water, extracted with THF. The organic layer was washed with brine, and dried with anhyd Na<sub>2</sub>SO<sub>4</sub>. Silica gel chromatographed with CH<sub>2</sub>Cl<sub>2</sub>-CH<sub>2</sub>Cl<sub>2</sub>:AcOH=40:1 to give target compound **1** (268 mg, 48 %) as red colored solid.

Physical data of **1**: Mp251-261°C.  $\delta_{\text{H}}$  (THF-*d*<sub>6</sub>, 500 MHz) 3.39 (s, 3H), 6.94 (t, J = 6.9 Hz, 1H), 7.07-7.18 (m, 3H), 7.34 (t, J = 7.0 Hz, 1H), 7.39 (t, J = 7.9 Hz, 1H), 7.65-7.72 (m, 3H), 8.92 (s, 1H).  $\delta_{\text{C}}$  (THF-*d*<sub>6</sub>, 125 MHz) 44.7, 112.8, 114.4, 116.9, 120.5, 123.9, 124.3, 125.6, 126.0, 126.8, 126.8, 127.2, 127.5, 127.8, 128.1, 131.1, 132.2, 132.4, 144.1, 146.9, 155.2, 163.2.;  $\nu$ (KBr) 1693 (C=O), 2230 (C≡N), cm<sup>-1</sup>; HRMS (FAB)  $m/z$  [M]<sup>+</sup>: calcd for C<sub>21</sub>H<sub>14</sub>O<sub>2</sub>N<sub>2</sub>S358.0776; found: 358.0748

(*E*)-2-cyano-3-(5-((*E*)-2-(12-methyl-12*H*-benzo[*b*]phenothiazin-11-yl)vinyl)thiophen-2-yl)acrylic acid **2**

A mixture of aldehyde **9** (420 mg, 1.05 mmol), cyanoacetic acid (117 mg, 1.37 mmol), ammonium acetate (25 mg, 1.32 mmol), and glacial acetic acid (70 mL) was heated at 90 °C for overnight in N<sub>2</sub> atmosphere. After reaction mixture was cooled, the reaction was quenched with water, extracted with THF. The organic layer was washed with brine, and dried with anhyd

Na<sub>2</sub>SO<sub>4</sub>. Silica gel chromatographed with CH<sub>2</sub>Cl<sub>2</sub>-CH<sub>2</sub>Cl<sub>2</sub>:AcOH=40:1 to give target compound **2** (342 mg, 70%) as red colored solid.

Physical data of **2**: Mp261-263°C (decomp.). δ<sub>H</sub> (CDCl<sub>3</sub>, 500 MHz) 3.44 (s, 3H), 6.84 (t, J = 15.9 Hz, 1H), 6.94 (t, J = 6.6 Hz, 1H), 7.00 (t, J = 7.6 Hz, 1H), 7.13-7.20 (m, 2H), 7.28-7.33 (m, 2H), 7.36 (t, J = 7.5 Hz, 1H), 7.58 (s, 1H), 7.64 (d, J = 7.3 Hz, 1H), 7.77-7.85 (m, 2H), 8.01 (d, J = 7.6 Hz, 1H), 8.38 (s, 1H). δ<sub>C</sub> (CDCl<sub>3</sub>, 100 MHz) 43.7, 100.2, 116.5, 118.8, 233.9, 123.9, 124.7, 125.3, 126.8, 127.0, 127.1, 127.8, 128.1, 128.3, 130.4, 131.2, 132.7, 133.8, 136.3, 139.8, 142.7, 146.4, 149.9, 152.6, 164.0.; ν(KBr) 1686 (C=O), 2220 (C≡N), cm<sup>-1</sup>; HRMS (FAB) m/z [M]<sup>+</sup>: calcd for C<sub>27</sub>H<sub>18</sub>O<sub>2</sub>N<sub>2</sub>S<sub>2</sub>466.0810; found: 466.0812

(*E*)-2-cyano-3-(5'-((*E*)-2-(12-methyl-12*H*-benzo[*b*]phenothiazin-11-yl)vinyl)-[2,2'-bithiophen]-5-yl)acrylic acid **3**

A mixture of aldehyde **12** (460 mg, 0.96 mmol), cyanoacetic acid (107 mg, 1.24 mmol), ammonium acetate (23 mg, 0.29 mmol), and glacial acetic acid (70 mL) was heated at 90 °C for overnight in N<sub>2</sub> atmosphere. After reaction mixture was cooled, the reaction was quenched with water, extracted with THF. The organic layer was washed with brine, and dried with anhydrous Na<sub>2</sub>SO<sub>4</sub>. Silica gel chromatographed with CH<sub>2</sub>Cl<sub>2</sub>-CH<sub>2</sub>Cl<sub>2</sub>:AcOH=40:1 to give target compound **3** (395 mg, 75%) as red colored solid.

Physical data of **3**: Mp226-228°C. δ<sub>H</sub> (CDCl<sub>3</sub>, 500 MHz) 3.45 (s, 3H), 6.75 (d, J = 15.7 Hz, 1H), 6.94 (t, J = 6.9 Hz, 1H), 7.01 (d, J = 7.5 Hz, 1H), 7.12-7.21 (m, 2H), 7.26-7.32 (m, 2H), 8.35 (t, J = 7.5 Hz, 1H), 7.44 (s, 1H), 7.47 (s, 1H), 7.54-7.60 (m, 2H), 7.64 (d, J = 7.4 Hz, 1H), 7.80 (s, 1H), 8.02 (d, J = 8.0 Hz, 1H), 8.35 (s, 1H). δ<sub>C</sub> (CDCl<sub>3</sub>, 125 MHz) 43.6, 100.0, 116.6, 118.8, 123.3, 123.8, 124.8, 125.0, 125.3, 125.6, 126.7, 127.1, 127.11, 127.2, 127.8, 128.0, 128.2, 128.4, 128.8, 129.0, 131.6, 132.8, 133.9, 135.8, 135.9, 140.1, 42.5, 146.2, 147.1, 149.1, 164.0. ; ν(KBr) 1686 (C=O), 2216 (C≡N), cm<sup>-1</sup>; HRMS (FAB) m/z [M]<sup>+</sup>: calcd for C<sub>31</sub>H<sub>20</sub>O<sub>2</sub>N<sub>2</sub>S<sub>3</sub>548.0687; found: 548.0680